

Comparison of Epitaxial and Textured Ferroelectric BaTiO₃ Thin Films

Baba Wague¹, Nicolas Baboux², Pedro Rojo Romeo¹, Yves Robach¹, Bertrand Vilquin¹

¹Université de Lyon, Ecole Centrale de Lyon, Institut des Nanotechnologies de Lyon, CNRS UMR, Ecully Cedex, France

²Université de Lyon, INSA de Lyon, Institut des Nanotechnologies de Lyon, CNRS UMR, Villeurbanne Cedex, France

Email: bertrand.vilquin@ec-lyon.fr

How to cite this paper: Wague, B., Baboux, N., Romeo, P.R., Robach, Y. and Vilquin, B. (2020) Comparison of Epitaxial and Textured Ferroelectric BaTiO₃ Thin Films. *Journal of Modern Physics*, 11, 509-516.

<https://doi.org/10.4236/jmp.2020.114033>

Received: February 27, 2020

Accepted: April 5, 2020

Published: April 8, 2020

Copyright © 2020 by author(s) and Scientific Research Publishing Inc. This work is licensed under the Creative Commons Attribution International License (CC BY 4.0).

<http://creativecommons.org/licenses/by/4.0/>



Open Access

Abstract

The properties of BaTiO₃ (BTO) thin films deposited on different substrates by RF magnetron sputtering were investigated. Two representative substrates were selected and different heterostructures were studied. 1) SrTiO₃ (STO) single crystals as a bulk oxide reference material, and 2) silicon as a semiconductor. SrRuO₃ (SRO) and Pt bottom electrodes were deposited on the silicon substrate. The BTO structural characterizations show that all the films have (001) crystallographic orientation. We have compared the electrical properties of the different samples: the same dielectric constant and polarization values were obtained independently of the nature of the substrate.

Keywords

Ferroelectric, Barium Titanate, Thin Film, Silicon, Sputtering, Epitaxy

1. Introduction

Among the ferroelectric perovskites, BaTiO₃ (BTO) has intensively been studied for a wide range of applications [1], MEMS devices [2], non-volatile memories, electro-optical devices [3], and piezoelectric and electro-optical properties [4]. Especially the fact that its composition is lead-free makes BTO very interesting for applications and many papers have discussed electrical and structural properties of BTO thin films [5] [6]. Various deposition techniques were used to grow thin films such as molecular beam epitaxy (MBE) [7] [8] [9], sol-gel deposition [10], pulsed laser deposition [11], chemical vapor deposition (CVD) [12], and RF sputtering [13] [14] [15]. RF sputtering is known to be one of the best compromises between deposition area size, stoichiometry, smoothness and de-

position speed problematics. High quality BTO thin films have generally been grown on lattice matched substrate such as MgO and SrTiO₃ (STO). In most cases, STO single-crystal is used as substrate as it also has a perovskite structure and its lattice parameters are close to those of BTO [16]. It is then easy to obtain epitaxially growth of BTO on STO. To check the electrical properties, conductive electrodes are needed. One can use a metal such as Pt, or a conductive oxide layer such as SrRuO₃ (SRO). The substrate and the bottom contact layer have to ensure good quality growth, and sufficient mechanical and thermal stabilities. In the present work, we investigate the structural and dielectric properties of 300 nm thick BTO thin films deposited by RF sputtering on different stacks of electrode/substrate: 1) SrRuO₃/SrTiO₃, 2) Pt/TiO₂/SiO₂/Si and 3) SrRuO₃/SrTiO₃/Si.

2. Experimental Procedure

In this work, the substrates were cleaned before performing the deposition process with acetone and ethanol in an ultrasonic bath. Firstly, bulk STO (001) and STO buffered Si (001) were used as a substrate to deposit the BTO/SRO. SRO (30 nm thick) was deposited with Ar/O₂ gas ratio = 10/1 at 4 mTorr and at 620°C. The STO buffer layer growth was performed by Molecular Beam Epitaxy on Si (004) wafer thanks to McKee process [17] [18]. Strontium was deposited on the native silica layer of the wafer and used for the reduction of SiO₂ and passivation layer on silicon, before the SrTiO₃ direct deposition around 360°C under oxygen atmosphere. Secondly, on Si (001) with native silica layer was deposited at room temperature by RF sputtering 120 nm-thick platinum bottom electrode. A thin TiO₂ layer (5 nm-thick) was used as buffer and adhesion layer between Pt and SiO₂. Then, the BTO thin films on all substrates were prepared by RF magnetron sputtering from a stoichiometric BaTiO₃ ceramic target. The deposition was carried out in gas ratio Ar/O₂ = 4/1 maintained at a pressure of 15 mTorr and a temperature of 650°C. After deposition, a rapid thermal annealing (RTA) at 650°C for 3 minutes under oxygen atmosphere was performed in order to reduce oxygen vacancies in BTO thin films and improve their structural and electrical properties. The crystalline nature of BTO thin films was checked by X-ray diffraction analysis with a Rigaku Smartlab diffractometer using CuK α radiation ($\lambda = 1.5406 \text{ \AA}$). For electrical measurements, platinum top electrodes (50 $\mu\text{m} \times 50 \mu\text{m}$ area and 250 nm-thick) were deposited by lift-off on all samples at room temperature. A sketch of the different samples can be found in **Figure 1**. To perform the capacitance-voltage (C-V) measurements, a HP 4284A precision

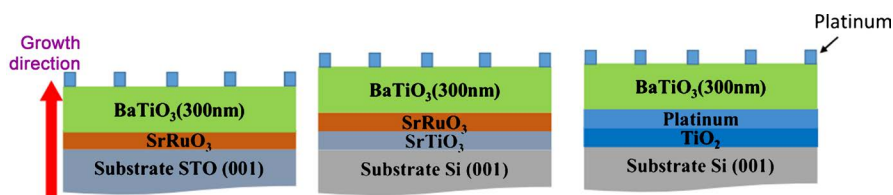


Figure 1. Schematic of the different samples. Pt top electrodes were deposited by lift-off at room temperature.

LCR meter was used. The ferroelectric hysteresis loops were evaluated with PUND (Positive Up Negative Down) method in order to extract the P-E hysteresis loop [19]. The PUND pulse train was programmed by LabView and a NF WF1966 2-channel generator. After application by a KEITHLEY 428 current amplifier, the current response was recorded by Nicolet INTEGRA-40 oscilloscope.

3. Results and Discussion

• Structural characterization

As a bulk material, BTO is normally crystallized in a tetragonal phase at room temperature. The difference between tetragonal phase and cubic phase in general is confirmed by the separation of diffraction peaks (002) and (200). **Figure 2(a)**, **Figure 2(c)** and **Figure 2(e)** show $2\theta/\omega$ patterns of 300 nm thick BTO grown on the different substrates. All diagrams indicate a preferential diffraction peak along the [001] direction, with no sign of secondary crystallographic orientation. Moreover, no other phase than the pure perovskite phase with a tetragonal structure is observed. The position corresponding to the 002 BTO reflection of bulk is obtained by angle determination ($2\theta = 44.86^\circ$). The BTO thin films on all substrates are *c*-oriented and strained with elongated *c*-axis. These results are consistent with experimental data from previous sputtering depositions [20]. The diffractograms for all samples are qualitatively similar: on ω scan, the rocking curves display a full width at half maximum (FWHM) between 1.16° and 1.36° , indicating the similar good crystallinity of BTO films, as shown in **Figure 2(b)**, **Figure 2(d)** and **Figure 2(f)**. These values are similar to those found in [21]. On the one hand, the phi-scan and reciprocal space mapping (RSM) patterns on the 103 reflections, shown in **Figure 3(a)** and **Figure 3(b)**, reveal the epitaxy of BTO films on bulk STO and STO buffered silicon substrates. The RSM measurements also show that the BTO films are relaxed on the substrates. On the other hand, the BTO deposited on Pt/TiO₂/SiO₂/Si is textured with out-of-plane *c*-axis. The $2\theta/\omega$ patterns allow calculating the out-of-plane *c*-parameter of BTO for all samples. Based on fitting of 002 reflection peaks, these *c*-parameter values are 4.07 Å, 4.06 Å and 4.03 Å (± 0.01 Å) respectively for BTO films deposited on BTO/SRO/STO and BTO/SRO/STO/Si and Pt/TiO₂/SiO₂/Si. This expansion of *c* parameter (bulk value of 4.038 Å) can be due to the epitaxial strain from the substrate for the epitaxial samples and/or the oxygen vacancies in BTO films. However, with a very low leakage current in the films (about 50 nA/cm² at 100 kV/cm applied field), it is expected that the films are vacancies-free. From RSM measurements, the in-plane *a*-parameter values were extracted and equal to 4.03 Å and 4.02 Å (± 0.01 Å) respectively for BTO/SRO/STO and BTO/SRO/STO/Si. Then, it was possible to calculate their $\frac{c}{a}$ ratio = 1.01 — equal to the bulk value one—which confirms the tetragonal structure of the BTO films. Although the substrates are different for BTO/SRO/STO and BTO/SRO/

STO/Si heterostructures, their structural properties are quite similar with same out-of-plane orientation and close lattice parameters.

• **Dielectric and ferroelectric properties**

Electrical and ferroelectric measurements were performed on the 3 samples. The investigation on the variation of the dielectric constant versus the applied

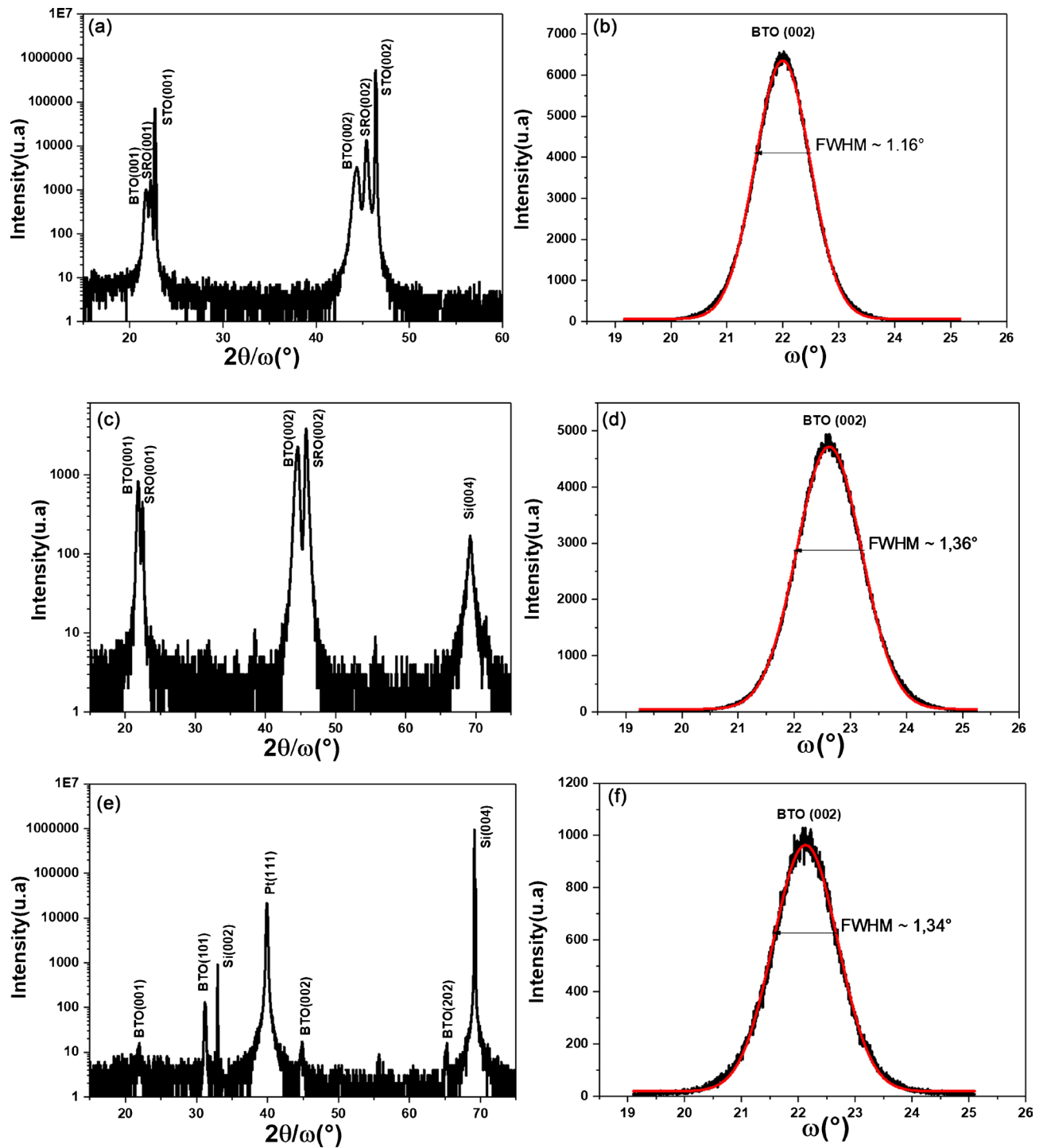


Figure 2. Out-of-plane XRD measurements of 300 nm thick BTO thin films on: (a) SRO/STO, (c) SRO/STO/Si and (e) Pt/TiO₂/SiO₂/Si. Rocking curve measurements around the BTO 002 respectively on (b) STO, (d) STO-Si and (f) Pt/TiO₂/SiO₂/Si.

electric field (C-V) is one of the methods for gaining insight into the behavior of the ferroelectric materials and has been used to characterize ferroelectric thin films [22] [23]. The C-V (Figure 4) characteristics measured on BTO films show the dielectric constant extracted from the small signal capacitance as a function of a DC bias voltage. The butterfly shape observed for all samples indicates the ferroelectric nature of the BTO tetragonal films. Very low leakage current (about 50 nA/cm^2 at 100 kV/cm applied field) was measured on the 3 samples. From Figure 4, the relative permittivity extracted using the parallel-plate capacitor equation was found $\epsilon_r = 115$ for all substrates, corresponding to its dielectric contribution. On all samples, we can observe a shift of the dielectric constant along the X-axis for positive values of the electric field. This can be explained by the fact that top and bottom electrodes were made of different materials, which

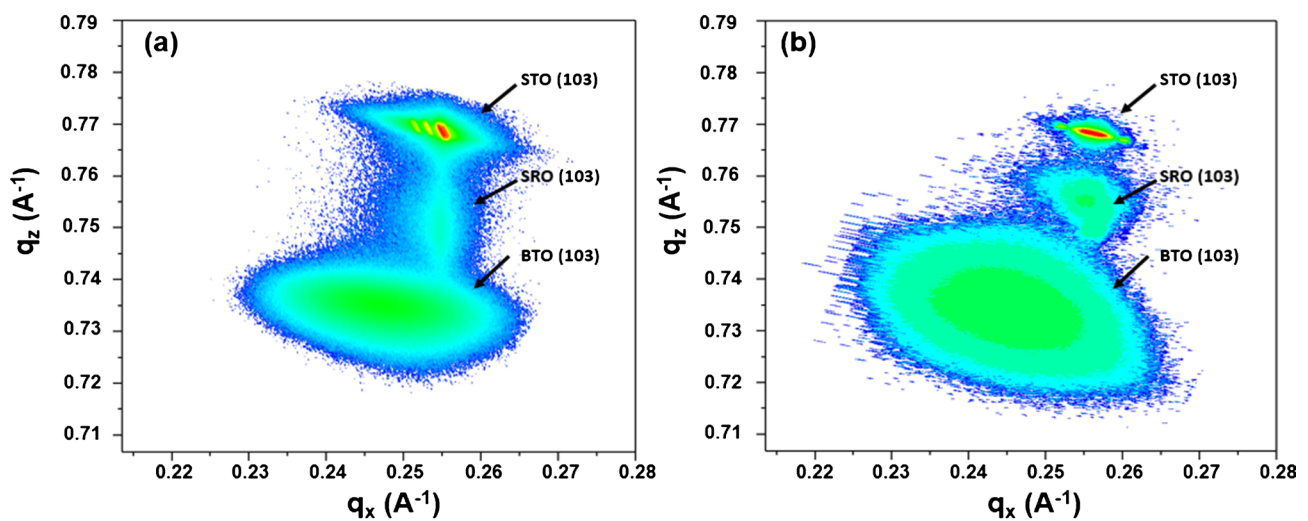


Figure 3. RSM measurements around the 103 STO, SRO and BTO reflections for BTO films deposited respectively on (a) STO substrate and (b) STO/Si template.

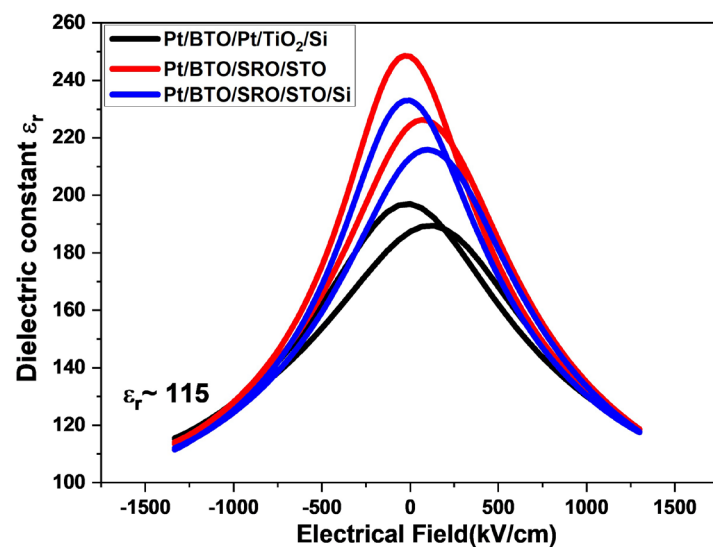


Figure 4. Dielectric constant curves of different samples: BTO/SRO/STO, BTO/SRO/STO/Si and BTO/Pt/TiO₂/SiO₂/Si.

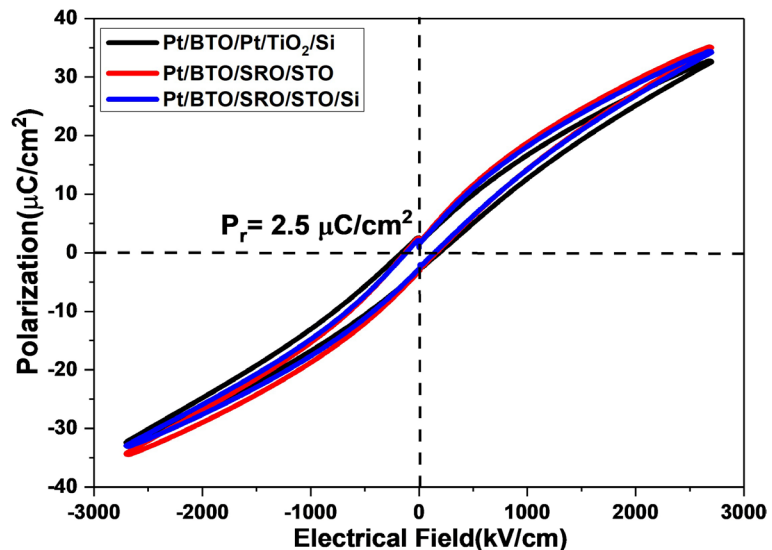


Figure 5. Ferroelectric hysteresis loops of different samples: BTO/SRO/STO, BTO/SRO/STO/Si and BTO/Pt/TiO₂/SiO₂/Si.

results in asymmetric properties of the upper and lower electrode-thin film interfaces, e.g. their work-function. The ferroelectric properties of BTO films on substrates were confirmed by hysteresis measurement as shown in **Figure 5**. It can be seen that all loops are normal P-E hysteresis ones. The corresponding remanent polarization value is $P_r = 2.5 \mu\text{C}/\text{cm}^2$ and the coercive field about $E_c = 170 \text{ kV}/\text{cm}$ for all samples. These results agree with other results close to state of art obtained for BTO films deposited by MOCVD [23] [24] [25] or sputtering [20] [26]. The small value of the P_r in BTO films can be due to the presence of space-charges within the films [26]. As all the BTO films have out-of-plane c-axis orientation, it is obvious that the remanent polarization and the coercive field are similar. In this work, the same values are obtained on all substrates. We obtained BTO films with similar out-of-plane structure and electrical properties regardless of the nature of the substrate. It seems that the same crystallization process by sputtering with post-deposition annealing under oxygen atmosphere used to realize all the samples leads to similar film properties independently of the nature of the substrate.

4. Conclusion

Ferroelectric BTO thin films were successfully deposited on bulk STO, STO- and Pt-buffered silicon substrates. We achieved epitaxial growth of BTO on STO and STO-buffered Si and texturation on Pt-buffered Si. The BTO films show similar electrical properties on the substrates used in this work (STO or Si). These results offer promise for low cost integration of ferroelectric BTO film on silicon wafer.

Acknowledgements

This work was realized on the Nanolyon technology platform. The authors thank Agence Nationale de la Recherche (funding grant ANR-14-CE26-0010—INTENSE

project), Region Rhone-Alpes (ARC4 funding grant) and GDR OXYFUN for their financial support.

Conflicts of Interest

The authors declare no conflicts of interest regarding the publication of this paper.

References

- [1] Roy, B.K. and Cho, J. (2012) *Journal of the American Ceramic Society*, **95**, 1189-1192. <https://doi.org/10.1111/j.1551-2916.2012.05104.x>
- [2] Bakhoun, E.G., Member, S. and Cheng, M.H.M. (2010) *Journal of Microelectromechanical Systems*, **19**, 443-450. <https://doi.org/10.1109/JMEMS.2010.2047632>
- [3] Dicken, M.J., Sweatlock, L.A., Pacifici, D., Lezec, H.J., Bhattacharya, K. and Atwater, H.A. (2008) *Nano Letters*, **8**, 4048-4052. <https://doi.org/10.1021/nl802981q>
- [4] Wang, D.Y., Wang, J., Chan, H.L.W. and Choy, C.L. (2007) *Integrated Ferroelectrics*, **88**, 12-20. <https://doi.org/10.1080/10584580601098522>
- [5] Beckers, L., Schubert, J., Zander, W., Ziesmann, J., Eckau, A., Leinenbach, P. and Buchal, C. (1998) *Journal of Applied Physics*, **83**, 3305-3310. <https://doi.org/10.1063/1.367099>
- [6] Kim, Y.S., Kim, D.H., Kim, J.D., Chang, Y.J., Noh, T.W., Kong, J.H., Char, K., Park, Y.D., Bu, S.D., Yoon, J.G. and Chung, J.S. (2005) *Applied Physics Letters*, **86**, Article ID: 102907. <https://doi.org/10.1063/1.1880443>
- [7] Niu, G., Yin, S., Saint-Girons, G., Gautier, B., Lecoœur, P., Pillard, V., Hollinger, G. and Vilquin, B. (2011) *Microelectronic Engineering*, **88**, 1232-1235. <https://doi.org/10.1016/j.mee.2011.03.028>
- [8] Niu, G., Gautier, B., Yin, S., Saint-Girons, G., Lecoœur, P., Pillard, V., Hollinger, G. and Vilquin, B. (2012) *Thin Solid Films*, **520**, 4595-4599. <https://doi.org/10.1016/j.tsf.2011.10.182>
- [9] Dubourdieu, C., Bruley, J., Arruda, T.M., Posadas, A., Jordan-Sweet, J., Frank, M.M., Cartier, E., Frank, D.J., Kalinin, S.V., Demkov, A.A. and Narayanan, V. (2013) *Nature Nanotechnology*, **8**, 748-754. <https://doi.org/10.1038/nnano.2013.192>
- [10] Sharma, H.B. and Mansingh, A. (1994) Sol-Gel Processed Barium Titanate Thin Films and Ceramics. *IEEE International Symposium on Applications of Ferroelectrics*, Vol. 4, 1385-1390.
- [11] García, T., Bartolo-Pérez, P., de Posada, E., Peña, J.L. and Villagrán-Muniz, M. (2006) *Surface and Coatings Technology*, **201**, 3621-3624. <https://doi.org/10.1016/j.surfcoat.2006.08.117>
- [12] Kim, T.W., Yoon, Y.S., Yom, S.S. and Kim, C.O. (1995) *Applied Surface Science*, **90**, 75-80. [https://doi.org/10.1016/0169-4332\(95\)00058-5](https://doi.org/10.1016/0169-4332(95)00058-5)
- [13] Nagatomo, T., Kosaka, T., Omori, S. and Omoto, O. (1981) *Ferroelectrics*, **37**, 681-684. <https://doi.org/10.1080/00150198108223520>
- [14] Zhang, W., Kang, L., Yuan, M., Yang, Q. and Ouyang, J. (2013) *Journal of Alloys and Compounds*, **580**, 363-368. <https://doi.org/10.1016/j.jallcom.2013.06.093>
- [15] Zhu, J.S., Lu, X.M., Jiang, W., Tian, W., Zhu, M., Zhang, M.S., Chen, X.B., Liu, X. and Wang, Y.N. (1997) *Journal of Applied Physics*, **81**, 1392. <https://doi.org/10.1063/1.363875>
- [16] Yang, Y., Priya, S., Wang, Y.U., Li, J. and Viehland, D. (2009) *Journal of Materials*

- Chemistry*, **28**, 4998-5002. <https://doi.org/10.1039/b903762d>
- [17] Niu, G., Saint-Girons, G., Vilquin, B., Delhay, G., Maurice, J.L., Botella, C., Robach, Y. and Hollinger, G. (2009) *Applied Physics Letters*, **95**, Article ID: 062902. <https://doi.org/10.1063/1.3193548>
- [18] Niu, G., Peng, W.W., Saint-Girons, G., Penuelas, J., Roy, P., Brubach, J.B., Maurice, J.L., Hollinger, G. and Vilquin, B. (2011) *Thin Solid Films*, **519**, 5722-5725. <https://doi.org/10.1016/j.tsf.2010.12.208>
- [19] Feng, S.M., Chai, Y.S., Zhu, J.L., Manivannan, N., Oh, Y.S., Wang, L.J., Yang, Y.S., Jin, C.Q. and Kim, K.H. (2010) *New Journal of Physics*, **12**, Article ID: 073006. <https://doi.org/10.1088/1367-2630/12/7/073006>
- [20] Zhang, W., Hu, F., Zhang, H. and Ouyang, J. (2017) *Materials Research Bulletin*, **95**, 23-29. <https://doi.org/10.1016/j.materresbull.2017.07.012>
- [21] El Marssi, M., Le Marrec, F., Lukyanchuk, I.A., Karkut, M.G., El Marssi, M., Le Marrec, F., Lukyanchuk, I.A. and Karkut, M.G. (2014) *Journal of Applied Physics*, **94**, 3307. <https://doi.org/10.1063/1.1596720>
- [22] Sreenivas, K., Mansingh, A. and Sayer, M. (1987) *Journal of Applied Physics*, **62**, 4475-4481. <https://doi.org/10.1063/1.339037>
- [23] Zeng, J., Wang, H., Wang, M., Shang, S., Wang, Z. and Lin, C. (1998) *Thin Solid Films*, **322**, 104-107. [https://doi.org/10.1016/S0040-6090\(97\)00965-6](https://doi.org/10.1016/S0040-6090(97)00965-6)
- [24] Stawski, T.M., Vijselaar, W.J.C., Göbel, O.F., Veldhuis, S.A., Smith, B.F., Blank, D.H.A. and Ten Elshof, J.E. (2012) *Thin Solid Films*, **520**, 4394-4401. <https://doi.org/10.1016/j.tsf.2012.02.029>
- [25] Yanase, N., Abe, K., Fukushima, N. and Kawakubo, T. (1999) *Journal of Applied Physics*, **38**, 5305-5308. <https://doi.org/10.1143/JJAP.38.5305>
- [26] Zhang, W., Gao, Y., Kang, L., Yuan, M., Yang, Q., Cheng, H., Pan, W. and Ouyang, J. (2015) *Acta Materialia*, **85**, 207-215. <https://doi.org/10.1016/j.actamat.2014.10.063>